Available online at http://ijcpe.uobaghdad.edu.iq and www.iasj.net
Iraqi Journal of Chemical and Petroleum Engineering
Vol. 24 No. 4 (December 2023) 59 – 73
EISSN: 2618-0707, PISSN: 1997-4884

Selecting Optimum Dimensions for a Three-Phase Horizontal Smart Separator for Khor Mor Gas-Condensate Processing Plant

Fenk A. Sulaiman [a, *], Hiwa Sidiq [b]

a Department of Petroleum Engineering, Faculty of Engineering, Soran University, Kurdistan Region, Iraq
b Department of Petroleum Engineering, Komar University of Science and Technology, Kurdistan Region, Iraq

Abstract

The Khor Mor gas-condensate processing plant in Iraq is currently facing operational challenges due to foaming issues in the sweetening tower caused by high-soluble hydrocarbon liquids entering the tower. The root cause of the problem could be liquid carry-over as the separation vessels within the plant fail to remove liquid droplets from the gas phase. This study employs Aspen HYSYS v.11 software to investigate the performance of the industrial three-phase horizontal separator, Bravo #2, located upstream of the Khor Mor sweetening tower, under both current and future operational conditions. The simulation results, regarding the size distribution of liquid droplets in the gas product and the efficiency gas/liquid separation, reveal that the separator falls short of eliminating all liquid droplets of specified sizes from the gas phase to meet efficiency requirements, weather with or without a mist extractor. Consequently, an analysis of various structural parameters of the vessel is undertaken to determine their impact on the carried-over liquid mass flow rate and the vessel's gas/liquid efficiency. The findings recommend a new design concept termed the "smart separator" for Bravo #2, applicable to both current and anticipated operational scenarios. The smart separator demonstrates a remarkable enhancement in gas/liquid separation efficiency, showcasing improvements of 21.31% and 24.02% under existing and future operating conditions, respectively. This innovative design proves effective in controlling liquid carry-over and maintaining high-efficiency levels, even as vessel inlet flow rates increase over time, thus preventing foaming phenomena in downstream processes caused carried-over liquids.

Keywords: Liquid carry-over, liquid droplet size distribution, gas/liquid separation efficiency, smart separator, adjustable weir plate, movable internal head.

Received on 09/07/2023, Received in Revised Form on 11/08/2023, Accepted on 12/08/2023, Published on 30/12/2023

https://doi.org/10.31699/IJCPE.2023.4.6

1- Introduction

Three-phase horizontal gravity separators are horizontally-oriented vessels that give space and the retention time to the produced fluid from the wells to disengage and separate into three different phases such as gas, light liquid (condensate if the well fluid is produced from a gas-condensate reservoir, or oil if the well fluid is produced from an oil reservoir), and heavy liquid (water) [1, 2]. They are generally the first processing vessels in surface facilities that were built to process high gas-liquid ratio mixtures, their inadequate sizing and internals make them operate inefficiently. In most cases, this results in increased liquid carry-over and subsequently diminishes the facility's total capacity. Downstream equipment cannot handle gas-liquid mixtures. For instance, compressors, dehydration towers, and sweetening towers need liquid-free gas, whereas pumps need gas-free liquid to stay out of cavitation [3]. To properly size a separator to give a high performance after choosing a seam-to-seam length and diameter using semiempirical techniques, it is crucial to use a software to study the performance of the newly sized vessels to verify their dimensions [4] because semiempirical ways could not predict the separation efficiency and they assume 100% of phase separation in their calculations [5–7].

Ahmed et al. [8] and Ghaffarkhah et al. [9] calculated various three-phase horizontal separator configurations using Arnold-Stewart and Monnery-Svrcek three-phase separator design semiempirical techniques. The derived geometries from each technique were then examined using computational fluid dynamics (CFD) simulations to evaluate their separation efficiency in terms of the separator outlet quality. Their simulation results indicated that the separator which was dimensioned using Arnold-Stewart technique, has a better separation efficiency than that was dimensioned by the Monnery-Svrcek technique. While, Carvalho et al. [10], Ahmed et al. [11], Khalifat et al. [12], Triwibowo et al. [13], Kharoua et al. [14], and Laleh et al. [15] used CFD simulations only to study the efficacy of the existing three-phase horizontal separators in different processing plants. The best choice to enhance the performance of an existing separator is to add new internals or replace the old ones with new ones. For instance, Kharoua et al. [16] used CFD simulations to

*Corresponding Author: Name: Fenk A. Sulaiman, Email: fenk.sulaiman@soran.edu.iq

conduct a proper design for new internals to increase the performance of a separator. A schoepentoeter device replaced the old momentum breaker, an agglomerator was positioned close to the gas outlet, two perforated plates were used to alter the internal flow behavior, and a battery of cyclones called spiral flow was used at the gas outlet. The CFD-based simulation predicted separation enhancement as a result of using the new set of internals. Conversely, for the undersized separators, adding new internals or replacing the old ones cannot increase the performance of the vessel and it has to be redesigned again as presented by Laleh et al. [17].

Despite that, as explained in the reviewed studies, the most common technique that had been used in selecting separator optimal dimensions, evaluating separator's separation efficiency, and debottlenecking the existing separators is *computational fluid dynamics*. This technique is a time-consuming process and requires very powerful computers. Alternatively, this case study applied the carry-over setup option correlations available within Aspen HYSYS software to assess the performance of the Bravo #2 separator. Subsequently, the impact of different vessel lengths, diameters, inlet nozzle sizes, weir heights, and light liquid (condensate) levels on the carried-over liquid mass flow rate and gas/liquid efficiency of the vessel were determined. Afterwards, the optimum dimensions were selected for the Bravo #2 separator under both current and future operating conditions. Ultimately, the dimensions chosen as optimal for the current operating conditions were combined with those identified for future conditions to construct the Bravo #2 smart separator. The smart separator configures an adjustable weir plate for controlling the liquid-gas interface height and a movable internal head for adjusting separator length based on varying feed flow rates.

2- Methodology

The Bravo #2 separator was simulated in static mode using Aspen HYSYS v.11 software, as illustrated in Fig. 1. The simulations aimed to assess the gas/liquid separation efficiency of the investigated vessel, improve its performance by incorporating new internals, determine the effect of vessel structural parameters on the carried-over liquid mass flow rate, and size Bravo #2 smart separator. Currently, inlet stream pressure, temperature, and molar flow rate of Bravo #2 are 7881 KPa, 29.9 °C, and 7979 Kgmole/h, respectively. In the near future, it is planned to increase the inlet molar flow rate to 8776.9 Kgmole/h. The inlet stream composition is detailed in Table 1.

2.1. Applied equation of state

To predict the phase behavior of the gas and liquid phases that occupied the vessel through the solution of fugacity parameters, the Soave-Redlich-Kwang (SRK) equation of state (EOS) was employed. Compared to the Peng-Robinson EOS, SRK is preferred for performing phase equilibrium calculations for various sour gases and gas condensates under different pressures and temperatures [18]. SRK equation of state which relates the pressure and temperature of the vessel with the molar volume of the components in the hydrocarbon mixture is presented as the following [19]:

$$P = \frac{RT}{v-b} - \frac{a}{v(v+b)} \quad (1)$$

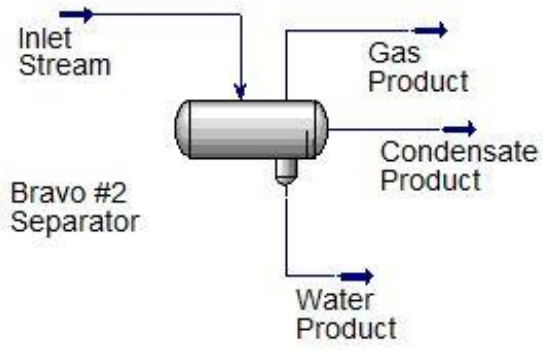

Fig. 1. Bravo #2 Separator Inside the Aspen HYSYS Software

Table 1. The Composition of the Inlet Mixture of Bravo #2 Separator

Components	Mole%	Components	Mole%
H_2O	0.172	n-Hexane	0.172
H_2S	0.010	Mcyclopentane	0.084
Nitrogen	0.194	Benzene	0.017
CO_2	0.179	Cyclohexane	0.058
Oxygen	0.010	Mcyclohexane	0.078
Methane	81.756	Toluene	0.060
Ethane	8.141	E-Benzene	0.014
Propane	4.206	m-Xylene	0.040
i-Butane	0.796	o-Xylene	0.013
n-Butane	1.780	Cumene	0.011
i-Pentane	0.545	C_{7+}	1.106
n-Pentane	0.557		
Molecular weight of C_{7+} component		141.7 gm/mol	
Density of C_{7+} component		767.0 Kg/m^3	

$$a = \sum_{i=1}^{N}\sum_{j=1}^{N} x_i x_j (a_i a_j)^{0.5}(1-k_{ij}),\ a_i = a_{ci}\,\alpha_i,\qquad a_{ci} = 0.427480\,R^2\frac{T_{ci}^2}{P_{ci}} \quad (2)$$

$a_{ci}\,\alpha_i$ together make up the attraction parameter, where α_i is the temperature dependence parameter. Likewise, α_i is expressed in Eq. 3 as relates pseudo-reduced temperature of the component *i* with the term m_i:

$$\alpha_i^{0.5} = 1 + m_i(1 - T_{ri}^{0.5}) \quad (3)$$

The term m_i is a function of the acentric factor of the component *i* as shown in the Eq. 4:

$$m_i = 0.480 + 1.574\,\omega_i - 0.176\omega_i \quad (4)$$

Al-Mhanna [20] proposed using the acentric factor as a standard to characterize both individual pure components

and common properties such as critical pressure, critical temperature, critical volume, and molecular weight. Similar to the coefficient a_{ci} , b_{ci} is a function of critical properties as expressed in Eq. 5 [19]:

$$b = \sum_{i=1}^{N} x_i b_{ci}\,, \qquad b_{ci} = 0.086640\, R\frac{T_{ci}}{P_{ci}} \tag{5}$$

SRK EOS can also be stated as a cubic equation in terms of compressibility (z) to differentiate between phases that are still in physical mixtures [21]:

$$z^3 - z^2 + (A - B - B^2)z - AB = 0 \tag{6}$$

The gas phase compressibility, z^g, is represented by the largest root, while the next z parameter corresponds to the next dense phase, and the smallest positive root represents the compressibility of the heaviest liquid phase, z^L. The dimensionless parameters A and B represent attraction and repulsion, respectively.

Olugbenga et al. [22] stated that fugacity is a valuable tool for analysing multicomponent equilibrium involving liquid and vapor phases. It enables the prediction of the reaction state and final phase of such mixtures at varying pressures and temperatures without the need for laboratory experiments. Additionally, it aids in managing deviations from ideal behavior in simulation and calculations. Eqs. 7 and 8 provide the partial fugacity and fugacity coefficient of component *i* in both the liquid and vapor phases [21].

$$ln\,\varphi_i^g = \frac{b_{ci}}{B}(z^g - 1) - ln(z^g - B) - \frac{A}{B}\left[\frac{b_{ci}}{B} - \frac{2}{a_{ci}\,a_i}\sum_j x_j\,(a\alpha)_{cij}\right] ln\left[\frac{z^g}{z^g - B}\right] f_i^g = x_i\,P\varphi_i^g \tag{7}$$

$$ln\,\varphi_i^L = \frac{b_{ci}}{B}(z^L - 1) - ln(z^L - B) - \frac{A}{B}\left[\frac{b_{ci}}{B} - \frac{2}{a_{ci}\,a_i}\sum_j x_j\,(a\alpha)_{cij}\right] ln\left[\frac{z^L}{z^L - B}\right] f_i^L = y_i\,P\varphi_i^L \tag{8}$$

The equilibrium ratio or the K-value of component *i* given by the following equation [21]:

$$k_i = \frac{y_i}{x_i} = \frac{\varphi_i^L}{\varphi_i^g} \tag{9}$$

When utilizing Eqs. 1 through 9 for a separation process, it is important to obtain the pauses parameter and begin at Eq. 9 and move upwards. This study employed the sequential substitution iteration (SSI) algorithm as documented. The computation process for flash using the SSI method to determine y_i, x_i, k_i, *L*, and *G* as follows [21]:

1. Equilibrium ratios of the components were expected from modified Wilson's equation which relates the pseudo-reduced pressure, pseudo-reduced temperature, and acentric factor of component *i* with the k_i:

$$k_i = P_{ri}^{-1}\, exp[5.37(\omega_i + 1)(1 - T_{ri}^{-1})] \tag{10}$$

2. The Rachford-Rice Equation was solved using Brent's method to calculate *G*.
3. The mole fractions of the liquid and gas components were then calculated.
4. Eq. 6 was utilized to solve for the compressibility of the gas and liquid phases, z^g and z^L, respectively.
5. The fugacity and fugacity coefficients for all components in the gas and liquid phases were computed.
6. The k_i values were updated using Eq. 11:

$$k_i = \frac{\varphi_i^L}{\varphi_i^g} \tag{11}$$

7. Steps 2 through 6 were repeated until Eqs. 12 and 13 was satisfied:

$$\varepsilon_f = \sum_{i=1}^{N}\left[\frac{f_i^L}{f_i^g} - 1\right]^2 < 10^{-15} \tag{12}$$

$$\varepsilon_g = [G - G^0]^2 < 10^{-15} \tag{13}$$

2.2. Carry-over correlations setup

In both steady state and dynamic simulations, real phase separation can be modelled with this option. Using the Correlation-based model, researchers may determine the expected carry-over based on the separator's inlet/exit device type, feed conditions, operating conditions, and vessel geometry. Three sets of correlations are available to calculate carried-over and carried-under droplet mass flow rates: Generic, Horizontal Vessel, and ProSeparator. The Horizontal Vessel correlations were established for horizontal three-phase separators. Six types of dispersions in the feed are being calculated for the inlet calculations using user-defined dispersion fractions and the expected efficiency of a user-defined inlet device. Then, for each dispersion excluding liquid/liquid dispersions, the user-supplied Rosin-Rammler parameters are used to compute the droplet distribution of the dispersed phase(s) [23].

The main gas/liquid separation is determined by dividing the residence time for the gas phase inside the vessel by the settling velocities for each liquid droplet size in the gas phase. If a droplet travels less vertically during its time inside the vessel than is necessary to rejoin its bulk phase, it is said to be carried over. Although the ProSeparator correlations are precise, they only account for liquid carry-over into gas and do not consider the inlet geometry. There aren't any estimates for gas entrainment or liquid/liquid separation in the liquid phases [23]. This case study selected Horizontal Vessel correlations to set up phase distributions at the inlet and predict liquid carry-over in gas/liquid separation and liquid/liquid separation sections. At the vapor exit section, the ProSeparator correlations were used to predict the droplet size distribution of carried-over liquids. The parameters which are written in Table 2 were entered into the Correlation Setup page.

The maximum droplet size of the dispersed liquid phases in the gas phase at the inlet was calculated mathematically by the user for both current and future inlet molar flow rates by applying a comprehensive

equation that considers all the physical properties of the gas and dispersed liquid phases, which is shown [15]:

$$d_{max} = 1.38\left(\frac{\sigma^{0.6}}{\rho_g{}^{0.3}\rho_d{}^{0.2}\mu_g{}^{0.1}}\right)\left(\frac{D_i^{0.5}}{u_i{}^{1.1}}\right)\times\left(1+0.5975\left[\frac{\mu_d(\mu_g{}^{0.25}u_i{}^{2.75}\rho_g{}^{-0.25}D_i^{-1.25}d_{max})^{\frac{1}{3}}}{\sigma}\right]\sqrt{\frac{\rho_g}{\rho_d}}\right)^{0.6} \quad (14)$$

The subscripts d and g are denoted as dispersed liquid and gas phases. The physical fluid properties of gas and dispersed liquid phases of the inlet stream illustrated in Table 2. Then d_{95} was calculated by the user from d_{max} for each dispersed phase by Eq. 15 and its corresponding values also are presented in Table 2:

$$d_{95} = 0.95\,(10^6)(d_{max}) \quad (15)$$

After the user gives d_{95} values for each dispersion to the Aspen HYSYS, it uses the Rosin-Rammler equation [12] to estimate the liquid droplet size distributions at the inlet gas phase of the separator:

$$Y_{(d)} = 1 - \exp(\frac{-d}{d_m})^n \quad (16)$$

Table 2. Inlet Holdup, Inlet Distribution Parameters, and Physical Properties of the Gas and Liquid Phases

Parameter	Value	Inlet distribution parameters	Physical fluid properties	
Liquid phase inversion (%)	10	Current operating conditions	Condensate/gas surface tension (N/m)	0.010
Liquid residence time factor	1	Condensate d_{95} dispersed in the gas phase (µm): 694 Water d_{95} dispersed in the gas phase (µm): 2026	Water/gas surface tension (N/m)	0.0712
Inlet condensate in the water phase (%)	13	Future operating conditions	The density of the gas phase (kg/m^3)	75.51
Inlet water in condensate phase (%)	10	Condensate d_{95} dispersed in the gas phase (µm): 625 Water d_{95} dispersed in the gas phase (µm): 1825	The density of the condensate phase (kg/m^3)	601.25
Inlet gas in condensate phase (%)	12	Note: In this research, the value of the Rosin-Rammler equation (n) spread parameter for all inlet liquid droplet size distributions was set in 2.	The density of the water phase (kg/m^3)	1004.8
Inlet gas in the water phase (%)	10		The viscosity of the gas phase (Pa. s)	1.41e^{-5}
			The viscosity of the condensate phase (Pa. s)	2.27e^{-4}
			The viscosity of the water phase (Pa. s)	7.97e^{-4}

The dimensions of the Bravo #2 vessel illustrated in Fig. 2 were inputted into the Dimensions Setup and DP/Nozzle Setup pages. The vessel is only equipped with a reverse distributor to lower the velocity and break down the momentum of the incoming three-phase fluid flow, which enters the vessel as a high-momentum stream. The condensate and water phase levels at current operating conditions were 0.45 and 0.25 m, respectively.

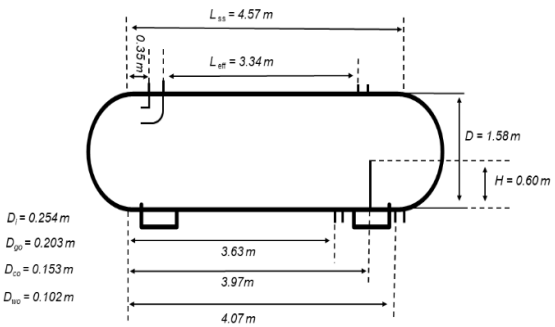

Fig. 2. The Geometrical Specifications of the Bravo #2 Separator

2.3. Carried-over liquid mass flow rate sensitivity

The structural parameter values employed to examine the sensitivity of the carried-over liquid mass flow rate in the gas product are outlined in Table 3. To calculate d_{max} and d_{95} for each inlet nozzle diameter, Eqs. 14 and 15 were utilized, and their corresponding d_{95} values are presented in Table 4. It is important to note that the selection of inlet nozzle diameters was based on industry standards and practical experience and was not chosen arbitrarily.

2.4. Bravo #2 smart separator sizing

Among the structural parameter values which are used to conduct carried-over liquid mas flow rate sensitivity, six different vessel configurations as presented in Table 5 were created to determine the optimal dimensions for the Bravo #2 separator under current operating conditions. The efficiency of each configuration was assessed in terms of the liquid droplet size distribution in the gas product. After the optimal configuration was determined to operate at the current conditions, an optimum effective length, weir height, and light liquid level were selected for future operating conditions based on liquid droplet

size distribution in the gas product. The resulting dimensions of optimal configuration for current operating conditions were combined with the optimal effective length, weir height, and condensate phase level for future conditions to construct Bravo #2 smart separator.

Table 3. The Structural Parameter Values of Carried-over Liquid Mass Flow Rate Sensitivity

The effective length of the vessel (m)	Diameter of the vessel (m)	Inlet nozzle diameter (m)	(Weir height (m), liquid light level (m))
5.01	2.212	0.478	(0.78, 0.585)
4.676	2.054	0.381	(0.72, 0.54)
4.342	1.896	0.303	(0.66, 0.495)
4.008	1.738	0.254	(0.6, 0.45)
3.674	1.58	0.202	(0.54, 0.405)
3.34	1.422	0.153	(0.48, 0.36)
3.006	1.264		(0.42, 0.315)
2.672	1.106		

Table 4. Corresponding Values of Condensate and Water d_{95} for Inlet Nozzle Diameters

Inlet nozzle diameter (m)	d_{95} for condensate droplets (μm)	d_{95} for water droplets (μm)
0.478	3818	11155
0.381	2072	6053
0.303	1117	3262
0.254	694	2026
0.202	374	1092
0.153	177	516

3- Results and Discussion

3.1. Model reliability

In order to validate the accuracy of the simulation model used in this study, the composition of the gas, condensate, and water products that were obtained from gas chromatography performed by CreDan Company laboratories was compared to product compositions gained from Aspen HYSYS simulation under current operating conditions. The comparison, as depicted in Fig. 3, reveals that there is only a minimal discrepancy between the mole percent of certain components of the composition of both gas products, indicating that the Aspen HYSYS software is a reliable and appropriate tool for simulating three-phase horizontal separators, assessing their gas/liquid separation efficiency, and predicting the amount of carried-over liquid mass flow rate within the gas phase. The slight observed difference in the mole percentage of certain constituents in the liquid product composition signifies that the model utilized also is dependable for evaluating liquid/liquid separation of the phases.

3.2. Gas/liquid separation efficiency evaluation

The Bravo #2 separator simulation results in terms of gas/liquid separation efficiency and droplet size distribution of condensate and water droplets in the gas product are applied to evaluate the efficiency of the investigated vessel, as shown in Table 6. In this study, the gas/liquid separation efficiency is defined as the ratio of the mass of the separated liquid droplets from the gas phase to the total mass of the dispersed liquid droplets at the inlet. The results affirm that the investigated vessel does not operate sufficiently because its efficiency in separating the liquid droplets from the gas phase is 79% for current operating conditions and 72% for future operating conditions. Moreover, the gas product stream holds the liquid droplets whose size equals 194 μm for the current conditions and 206 μm for future conditions. For a three-phase horizontal separator that is not equipped with an exit mist extractor device, it is required to operate at a gas/liquid separation efficiency of over 80% [24, 25] and remove all the liquid droplets in the gas product whose size is equal to and greater than 100 μm [5, 6].

Table 5. Set of proposed vessel configurations for Bravo #2 separator for the current operating conditions

	Case 1	Case 2	Case 3	Case 4	Case 5	Case 6
The effective length of the vessel for gas/liquid separation (m)	5.01	4.008	5.01	5.01	4.342	4.342
Seam-to-seam length of the vessel (m)	6.688	5.686	6.494	6.494	6.02	5.826
Diameter of the vessel (m)	2.212	2.212	2.212	2.054	2.212	2.212
Inlet nozzle diameter (m)	0.478	0.478	0.381	0.381	0.478	0.381
Inlet nozzle location (m)	0.35	0.35	0.35	0.35	0.35	0.35
Weir height (m)	0.54	0.54	0.54	0.54	0.54	0.54
Condensate phase level (m)	0.405	0.405	0.405	0.405	0.405	0.405
Weir location (m)	3.97	3.97	3.97	3.97	3.97	3.97
Condensate outlet nozzle diameter (m)	0.153	0.153	0.153	0.153	0.153	0.153
Condensate outlet nozzle location (m)	4.07	4.07	4.07	4.07	4.07	4.07
Water outlet nozzle diameter (m)	0.102	0.102	0.102	0.102	0.102	0.102
Water outlet nozzle location (m)	3.63	3.63	3.63	3.63	3.63	3.63
Slenderness ratio (L_{ss}/D)	3.02	2.57	2.94	3.16	2.72	2.63

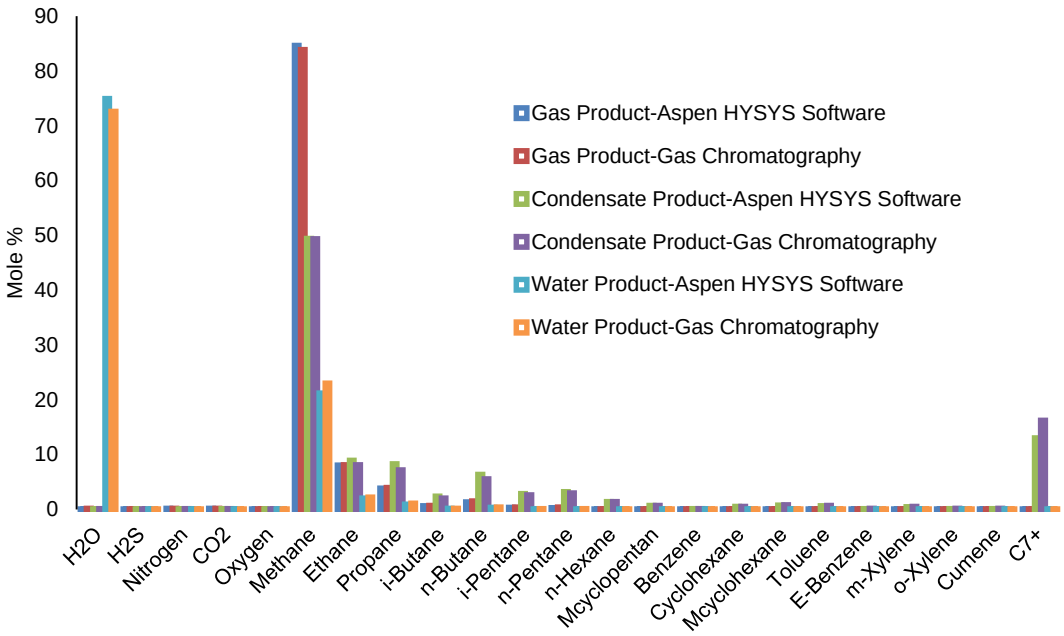

Fig. 3. The Composition of the Gas, Condensate, and Water Products of Bravo #2 Separator that Was Determined by Gas Chromatography and Aspen HYSYS Software under Current Operating Conditions

Table 6. Droplet Size Distribution of Condensate and Water Droplets at the Gas Product at the Current and Future Operating Conditions

Current operating conditions				Future operating conditions			
Condensate droplets		Water droplets		Condensate droplets		Water droplets	
Size (μm)	Mass percent (%)	Size (μm)	Mass percent (%)	Size (μm)	Mass percent (%)	Size (μm)	Mass percent (%)
0.69	0.0014	2	0.02	0.63	0.00105	2	0.01
7	0.25	20	4.33	6	0.19	18	2.53
14	0.55	41	9.62	13	0.42	36	5.62
21	0.83	61	14.40	19	0.63	55	8.42
28	1.10	81	19.16	25	0.84	73	11.21
35	1.38	101	23.89	31	1.04	91	13.97
42	1.65	122	28.57	38	1.25	109	16.71
49	1.91			44	1.45	128	19.42
56	2.18			50	1.65	146	22.10
62	2.44			56	1.84		
69	2.69			63	2.04		
76	2.94			69	2.23		
83	3.19			75	2.41		
90	3.43			81	2.59		
97	3.66			88	2.77		
104	3.89			94	2.94		
111	4.11			100	3.11		
118	4.33			106	3.27		
125	4.53			113	3.43		
132	4.73			119	3.58		
139	4.92			125	3.72		
146	5.11			131	3.86		
153	5.28			138	4.00		
160	5.45			144	4.12		
167	5.61			150	4.24		
174	5.75			156	4.35		
180	5.89			163	4.46		
187	6.02			169	4.56		
194	6.14			175	4.65		
				181	4.73		
				188	4.81		
				194	4.88		
				200	4.94		
				206	5.00		

Installing a mist extractor device is one of the most effective methods to enhance the gas/liquid separation efficiency of an existing three-phase horizontal separator that lacks a mist eliminator device. After adding a

standard wire mesh mist extractor with a pad thickness of 101.4 mm, wire diameter of 0.28 mm, and specific surface area of 360 m^2/m^3 [26, 27], the simulation results for the Bravo #2 separator under current and future conditions in terms of liquid droplet size distribution in the gas product are presented in Table 7. However, the results indicate that the Bravo #2 separator still fails to produce a gas product that meets the required gas quality due to the high mass percentage of water droplets with sizes equal to and greater than 20 μm. To meet the gas quality guideline of 0.013 m^3/MMm^3 (0.1 gal/MMscf) [3, 5, 28], a mist eliminator device must remove all liquid droplets larger than 20 μm [29] from the gas phase.

Table 7. Droplet Size Distribution of Condensate and Water Droplets at the Gas Product at the Current and Future Operating Conditions after Installing the Mist Extractor Device

Current operating conditions				Future operating conditions			
Condensate droplets		Water droplets		Condensate droplets		Water droplets	
Size (μm)	Mass percent (%)	Size (μm)	Mass percent (%)	Size (μm)	Mass percent (%)	Size (μm)	Mass percent (%)
0.69	0.47	2	51.42	0.63	0.42	2	41.19
7	70.45	20	21.56	6	64.95	18	23.41
14	21.37	41	4.91	13	25.39	36	4.35
21	2.52	61	4.53	19	3.21	55	3.80
28	0.65	81	5.07	25	0.77	73	4.17
35	0.32	101	5.83	31	0.35	91	4.75
42	0.22	122	6.68	38	0.23	109	5.41
49	0.18			44	0.18	128	6.10
56	0.16			50	0.16	146	6.81
62	0.15			56	0.15		
69	0.15			63	0.14		
76	0.15			69	0.14		
83	0.15			75	0.14		
90	0.16			81	0.14		
97	0.16			88	0.15		
104	0.16			94	0.15		
111	0.17			100	0.15		
118	0.17			106	0.16		
125	0.18			113	0.16		
132	0.18			119	0.17		
139	0.19			125	0.17		
146	0.19			131	0.17		
153	0.20			138	0.18		
160	0.20			144	0.18		
167	0.21			150	0.19		
174	0.21			156	0.19		
180	0.21			163	0.19		
187	0.22			169	0.20		
194	0.22			175	0.20		
				181	0.20		
				188	0.20		
				194	0.21		
				200	0.21		
				206	0.21		

3.3. Carried-over liquid mass flow rate sensitivity analysis

3.3.1. The impact of the vessel effective length

Based on the findings presented in Fig. 4, it can be observed that increasing the effective length of the vessel from 3.34 to 5.01 m leads to a decrease in the mass flow rate of carried liquid within the gas phase from 853.39 to 425.13 Kg/h and an improvement in gas/liquid separation efficiency by 10%. This phenomenon occurs because longer vessels provide more residence time for the gas phase, allowing smaller liquid droplets to settle more effectively under the influence of gravity. Settling of finer droplets takes more time to cross the required vertical distance to reach the gas/liquid surface than the coarser droplets.

3.3.2. The impact of the vessel diameter

Fig. 5 demonstrates that increasing the vessel diameter from 1.58 to 2.212 m eliminates the mass flow rate of carried liquid in the gas product from 853.39 to 467.21 Kg/h and improves the gas/liquid separation efficiency of the separator by 9%. This is because vessels with larger diameters provide a greater surface area and slower gas phase velocities, allowing smaller liquid droplets sufficient time to coalesce and reach the gas/condensate interface [9]. Although smaller diameter vessels may be more cost-effective, they must be inspected for potential liquid re-entrainment in the gas phase and disturbance of the gas/liquid interface.

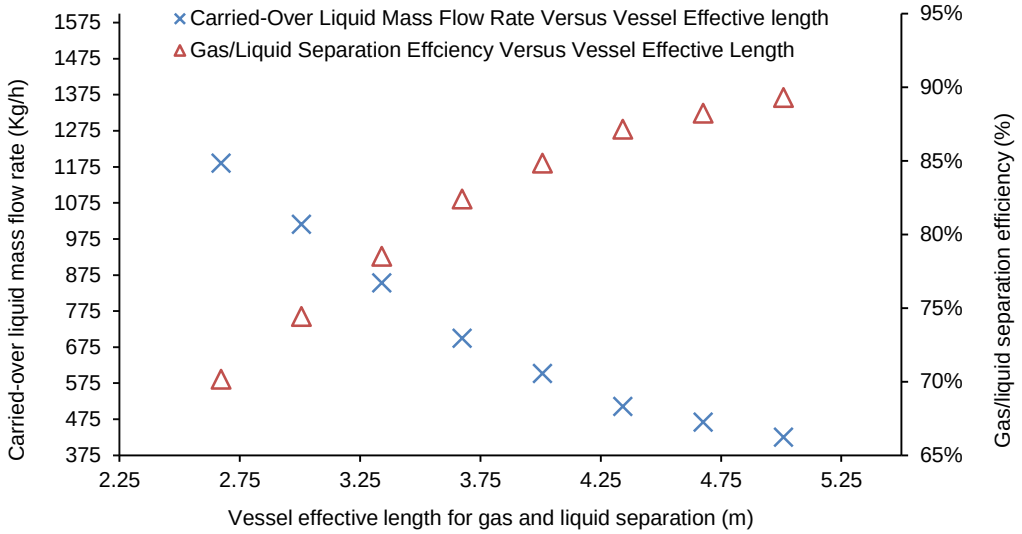

Fig. 4. Carried-over Liquid Mass Flow Rate and Gas/Liquid Separation Efficiency versus the Vessel Effective Length

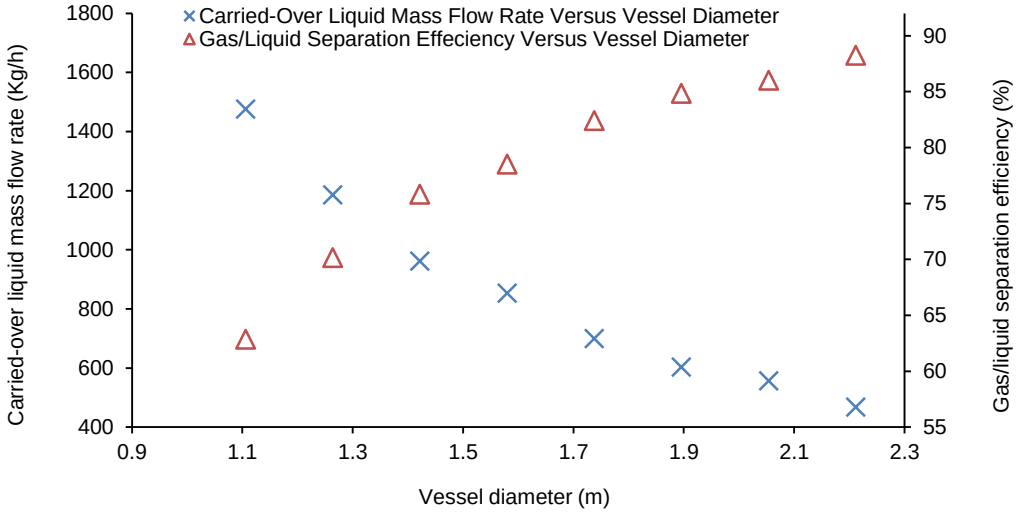

Fig. 5. Carried-over Liquid Mass Flow Rate and Gas/Liquid Separation Efficiency versus the Vessel Diameter

3.3.3. The impact of the inlet nozzle size

By examining Fig. 6, it can be detected that an increase in the inlet nozzle diameter of the vessel from 0.254 to 0.478 m results in a reduction in the mass flow rate of the carried liquid with the gas product from 853.39 to 35.13 Kg/h. Additionally, the separator's gas/liquid separation efficiency improves by 20%. This is because separators with smaller inlet nozzle diameters can generate higher velocities and turbulence, leading to finer liquid droplet size distributions at the inlet [30]. Finer liquid droplet size distributions are more likely to pass through the vessel and exit with the gas product. Out of all the vessel structural parameters investigated in this research, the inlet nozzle size has the most significant impact on liquid carry-over and vessel efficiency.

3.3.4. The impact of the weir height and condensate phase level

Based on Fig. 7, it can be seen that reducing the weir height from 0.60 to 0.54 m and condensate phase level from 0.45 to 0.405 m results in a decrease in the mass flow rate of the carried liquid with the gas product from 853.39 to 800.97 Kg/h and only a slight improvement in the gas/liquid separation efficiency of the separator by 1%. This is because separators with shorter weir heights and lower gas/liquid interfaces result in lower velocities for the gas phase to pass through the vessel, which allows finer liquid droplets more time to reach the gas/liquid interface [16].

3.4 Bravo #2 smart separator optimum dimensions

Table 8 presents the simulation results for the liquid droplet size distribution in the gas product of various proposed configurations for the Bravo #2 separator at the current conditions, in order to select the optimal vessel dimensions. The results indicate that Case 1 and Case 3 could remove all liquid droplets in the gas phase that were equal to or larger than 100 µm, but their effective lengths were higher compared to Case 5. Case 2 did not have a sufficient effective length to remove all the required

liquid droplets. On the other hand, Case 4 and Case 6 were unable to remove all the liquid droplets of interest. Therefore, Case 5, as shown in Fig. 8, was selected as the optimal vessel configuration for the Bravo #2 separator at the current condition, as it could effectively remove all the liquid droplets of interest from the gas phase, and its slenderness ratio (ratio of seam-to-seam vessel length to vessel diameter) of 2.72 fell within the range proposed by Smith [3] of 2-6. According to Ghaffarkhah et al. [31], the range proposed by Smith [3] is the most suitable range for designing the optimal vessel configuration for high-gas-content fluids, and separators with lower slenderness ratios perform better.

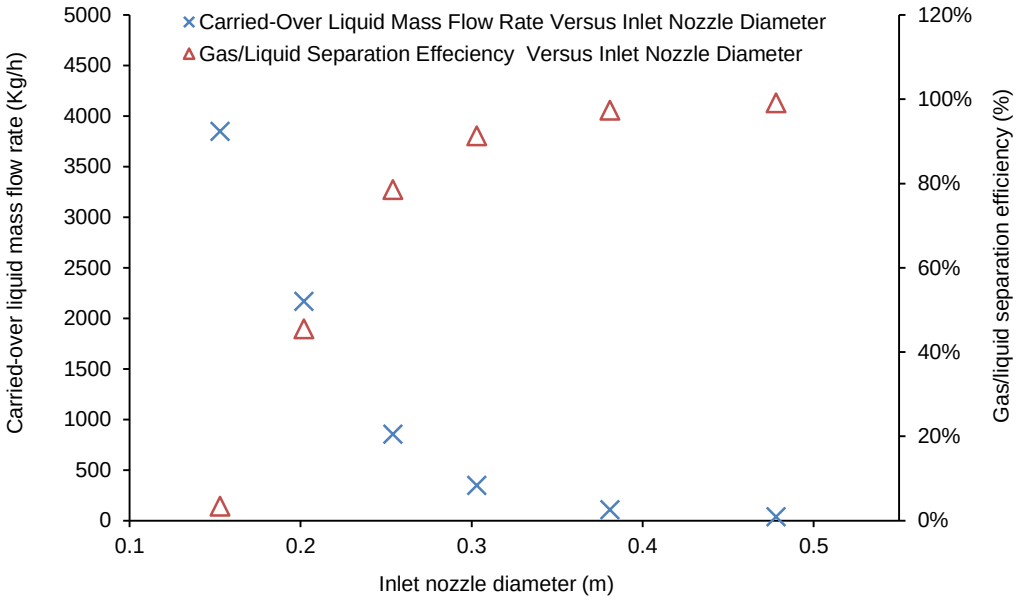

Fig. 6. Carried-over Liquid Mass Flow Rate and Gas/Liquid Separation Efficiency versus Inlet Nozzle Diameter of the Vessel

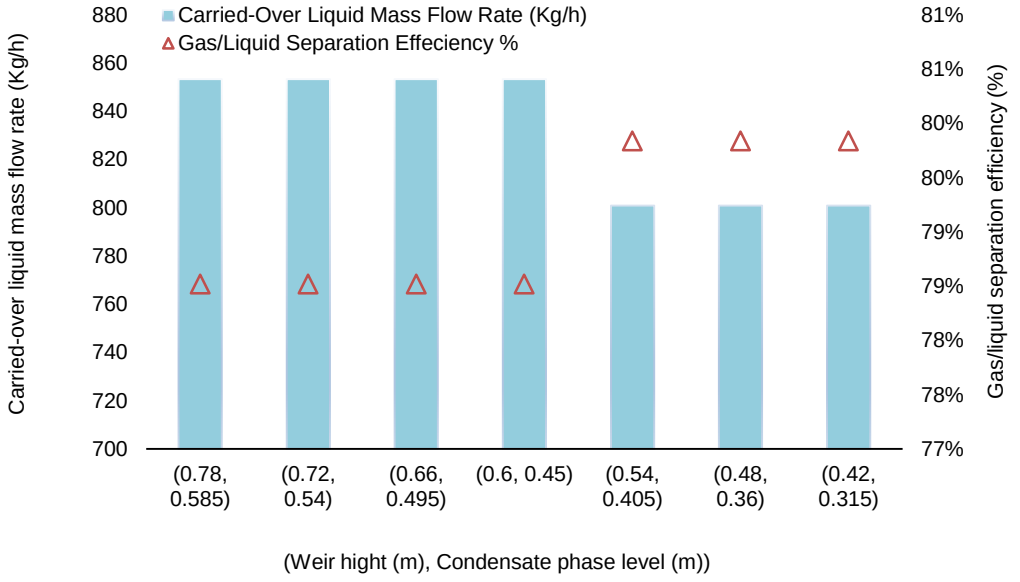

Fig. 7. Carried-over Liquid Mass Flow Rate and Gas/Liquid Separation Efficiency versus Weir Height and Condensate Phase Level of the Vessel

Table 8. Liquid Droplet Size Distribution in the Gas Product of Various Proposed Configurations for the Bravo #2 Separator for the Current Conditions

Case 1				Case 2			
Condensate droplets		Water droplets		Condensate droplets		Water droplets	
Size (µm)	Mass percent (%)	Size (µm)	Mass percent (%)	Size (µm)	Mass percent (%)	Size (µm)	Mass percent (%)
4	0.17	10	100	4	0.08	10	100
38	31.00			38	15.26		
76	68.83			76	33.89		
				115	50.76		
Case 3				Case 4			
Condensate droplets		Water droplets		Condensate droplets		Water droplets	
Size (µm)	Mass percent (%)	Size (µm)	Mass percent (%)	Size (µm)	Mass percent (%)	Size (µm)	Mass percent (%)
2	0.05	6	0.55	2	0.03	6	0.55
20	9.11	60	99.45	20	6.06	60	99.45
40	20.23			40	13.46		
60	30.30			60	20.16		
80	40.31			80	26.83		
				100	33.45		
Case 5				Case 6			
Condensate droplets		Water droplets		Condensate droplets		Water droplets	
Size (µm)	Mass percent (%)	Size (µm)	Mass percent (%)	Size (µm)	Mass percent (%)	Size (µm)	Mass percent (%)
4	0.17	10	100	2	0.03	6	0.55
38	31.00			21	6.06	61	99.45
76	68.83			42	13.46		
				63	20.16		
				84	26.83		
				105	33.45		

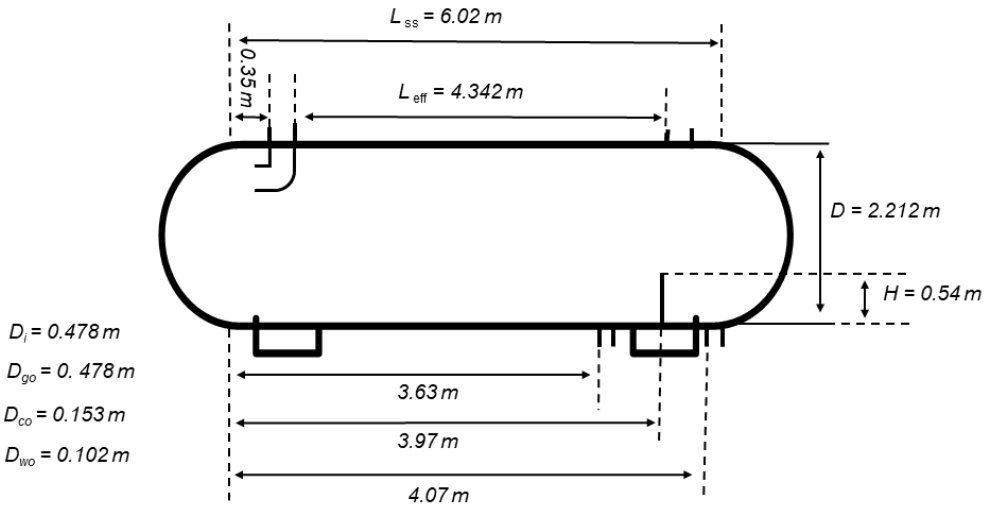

Fig. 8. The Optimum Vessel Configuration for the Current Operating Conditions

Moreover, the optimum vessel dimensions to operate in the future are shown in Fig. 9 and the liquid droplet size distribution in its gas product is demonstrated in Table 9. The selected dimensions were based on the liquid droplet size distribution in the gas product, which indicated that this vessel configuration could effectively remove all liquid droplets that were equal to or larger than 100 µm in size. Most optimal dimensions remain similar to the vessel configuration selected for current conditions, except for an increase in length and a decrease in weir plate height. The resulting slenderness ratio of the vessel is 3.14, which falls within the range proposed by Smith [3].

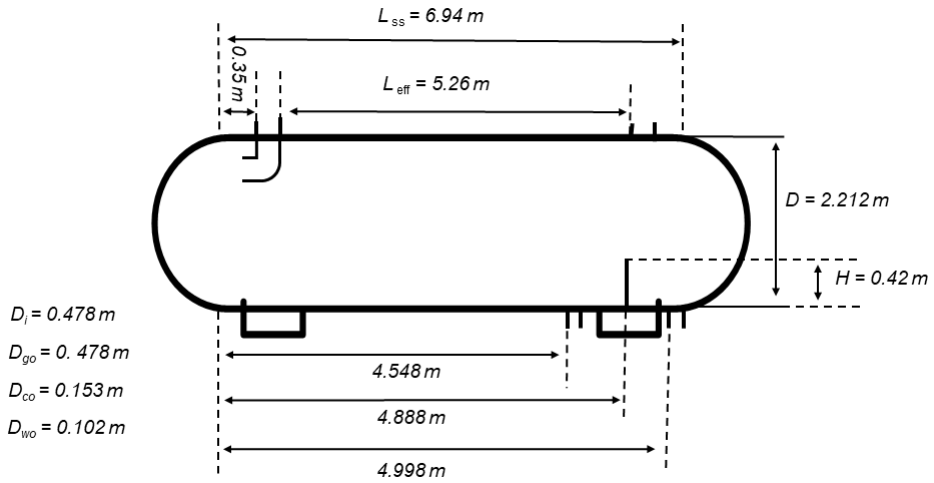

Fig. 9. The Optimum Vessel Configuration for the Future Operating Conditions

Table 9. Liquid Droplet Size Distribution in the Gas Product of the Optimum Vessel Configuration for the Future Operating Conditions

Condensate droplets		Water droplets	
Size (μm)	Mass percent (%)	Size (μm)	Mass percent (%)
3.4	0.17	10	100
34	31.00		
68	68.83		

The optimal vessel configuration selected for the current operating conditions was combined with the optimum vessel dimensions designed for future operating conditions to build Bravo #2 smart separator, the dimensions of which are illustrated in Fig. 10. The smart design can handle different inlet flow rates effectively by adjusting its length and weir plate height. For example, it can efficiently separate 7979 Kgmole/h of inlet mixture at the current conditions with a seam-to-seam length of 6.02 m and a weir plate height of 0.54 m. Additionally, it maintains its high performance and can effectively separate 8776.9 Kgmole/h of inlet mixture in the future when its seam-to-seam length is increased from 6.02 to 6.94 m by moving its movable internal head to the left-hand side and decreasing the weir plate height from 0.54 to 0.42 m. For the current operating conditions, the inlet mixture enters the vessel through *N2*, while for future operating conditions, the inlet mixture enters the vessel through a bypass to *N1*. The inlet diverter device is welded onto the movable internal head to move with the head and fit with *N1* when the vessel operates in future conditions.

The smart design may be considered an ideal design that can control liquid carry-over and maintain high efficiency as the inlet flow rate increases over time, thereby avoiding overload on the inlet scrubbers and foam generation in the downstream processes due to liquid carry-over. Inlet scrubbers can experience overload when the mass flow rate of the carried-over liquid is high, or the ambient temperature drops, particularly in cold environments. Occasionally, ambient temperature reductions and high carried-over liquid rates may occur simultaneously. In such circumstances, the smart design can regulate liquid carry-over and collaborate with inlet scrubbers to reduce the load and maintain the downstream processes' performance. This design is especially suitable for gas-condensate processing plants, as they are highly sensitive to operational changes and environmental conditions.

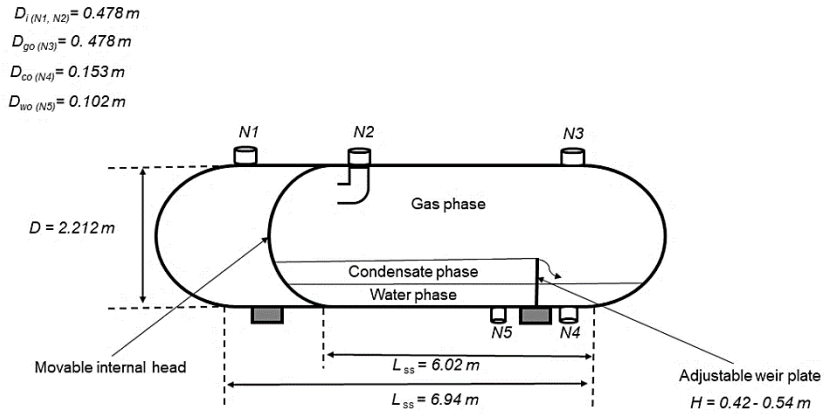

Fig. 10. Bravo #2 Smart Separator

4- Conclusions

This research employed the carry-over correlations option in Aspen HYSYS to identify the optimal configuration for a smart separator to replace the Bravo #2 separator in the Khor Mor gas-condensate processing plant. The main objective was to manage liquid carry-over and prevent foaming phenomena in the downstream gas sweetening tower. The key findings of this study can be summarized as follows:

1. The utilization of carry-over correlations proves to be reliable and efficient approach for assessing the separator performance and determining optimal dimensions.
2. Increasing the effective length and diameter of the vessel reduces the mass flow rate of carried liquid within the gas phase, thereby enhancing the gas/liquid separation efficiency.
3. Larger inlet nozzle diameters lead to a decrease in velocity/turbulence of the separator's feed, resulting in larger liquid droplets/gas bubbles. this enhancement promotes liquid/gas gravity separation, reduces carried-over liquid flow rate, and improves overall gas/liquid separation efficiency. Notably, the inlet nozzle size exhibits the most significant impact on the separator's efficiency compared to other studied parameters.
4. Shorter plate weirs contribute to lower the height of the gas/liquid interface, subsequently reducing carried-over liquid rates.
5. The smart separator emerges as a practical solution for operational changes, featuring an adjustable plate weir to control the liquid-gas interface's height and a movable internal head to adjust the separator's length based on varying inlet flow rates.

Acknowledgments

The industrial data utilized in this study was provided by CreDan, the company that owns the Khor Mor gas-condensate processing plant. The authors would like to express their gratitude towards CreDan for their contribution.

Nomenclatures

A Attraction parameter
a_{ci} Pressure correction parameter for the intermolecular forces of attraction, J.m^3/mol^2
B Repulsion parameter
b_{ci} Molar volume parameter for the correction of volume, m^3/mol
D Internal diameter of the vessel, m
D_i Internal diameter of the inlet nozzle, m
D_{go} Internal diameter of the gas phase outlet nozzle, m
D_{co} Internal diameter of the condensate phase outlet nozzle, m
D_{wo} Internal diameter of the water phase outlet nozzle, m
d_{max} Maximum droplet size of the dispersed phase, m
d_{95} 95% of droplets are smaller than this diameter for the specified dispersion, µm
d_m Mean diameter for the specified distribution, µm
f_i Partial fugacity of *i* component
H Height of the weir plate, m
k_{ij} Binary interaction parameter between components *i* and *j*
k_i Equilibrium constant of *i* component
L Number of moles of the hydrocarbon mixture in the liquid phase
L_{ss} Seam-to-Seam length of the vessel, m
L_{eff} The length of the vessel where separation takes place effectively, m
N Number of components in the hydrocarbon mixture
n Spread parameter of the Rosin-Rammler equation
P Operating pressure of the vessel, KPa
P_{ci} Critical pressure of the *i* component, KPa
P_{ri} Reduced pressure of the *i* component
R Gas constant, KPa.m^3/mol.^{o}C
T Operating temperature of the vessel, ^{o}C
T_{ci} Critical temperature of the *i* component, ^{o}C
T_{ri} Reduced temperature of the *i* component
u_i Velocity of the inlet mixture, m/s
G Number of moles of the hydrocarbon mixture in the gas phase
v Molar volume, m^3/mol
x_i Liquid mole fraction of *i* component
y_i Vapor mole fraction of *i* component
$Y_{(d)}$ Mass fraction of droplets, %
z^g Compressibility of the gas phase
z^L Compressibility of the heaviest liquid phase

Greek Letters

α_i Temperature dependence parameter
ε_g Convergence tolerance for fugacity of gas
ε_f Convergence tolerance for fugacity of fluid
μ_g Viscosity of the gas phase, Pa.s
μ_d Viscosity of the dispersed droplet in the gas phase, Pa.s
ρ_g Density of the gas phase, kg/m^3
ρ_d Density of the dispersed droplet in the gas phase, kg/m^3
ω_i Acentric factor of the *i* component
φ_i Fugacity coefficient
σ Surface tension of the dispersed droplet, N/m

References

[1] S. Mokhatab, W. A. Poe, and J. Y. Mak, *Handbook of natural gas transmission and processing: Principles and practices*, Fourth. Gulf Professional Publishing, Cambridge, USA, 2018.
[2] G. madeeh Al-Zubaidy, "Determining Optimum Oil Separator Size and Optimum Operating Pressure," *Iraqi J. Chem. Pet. Eng.*, vol. 23, no. 2, pp. 43–46, 2022, https://doi.org/10.31699/IJCPE.2022.2.6

[3] H. V. Smith, "Oil and Gas Separators.," in *Petroleum Engineering Handbook*, Third Edit., H. B. Bradley, Ed. Society of Petroleum Engineers, Richardson, TX, U.S.A., 1987.

[4] A. Ghaffarkhah, Z. A. Dijvejin, M. A. Shahrabi, M. K. Moraveji, and M. Mostofi, "Coupling of CFD and semiempirical methods for designing three-phase condensate separator: case study and experimental validation," *J. Pet. Explor. Prod. Technol.*, vol. 9, no. 1, pp. 353–382, 2019, https://doi.org/10.1007/s13202-018-0460-5

[5] A. Bahadori, *Natural Gas Processing Technology and Engineering Design*. Gulf Professional Publishing,Waltham, USA, 2014.

[6] M. Arnold and K., Stewart, *Surface Production Operations-Design of Oil Handling Systems and Facilities*, Third. Gulf Professional Publishing, Burlington, USA, 2008.

[7] W. Y. Monnery and W.D., Svrcek, "Successfully Specify Three-Phase Separators," *Chem. Eng. Prog.*, no. 90, pp. 29–40, 1994.

[8] T. Ahmed, F. Hamad, and P. A. Russell, "The use of CFD simulations to compare and evaluate different sizing algorithms for three-phase separators," in *Offshore Technology Conference Brasil*, 2017, pp. 1051–1066, https://doi.org/10.4043/28066-ms

[9] A. Ghaffarkhah, M. Ameri Shahrabi, M. Keshavarz Moraveji, and H. Eslami, "Application of CFD for designing conventional three phase oilfield separator," *Egypt. J. Pet.*, vol. 26, no. 2, pp. 413–420, 2017, https://doi.org/10.1016/j.ejpe.2016.06.003

[10] A. J. G. Carvalho, D. C. Galindo, M. S. C. Tenório, and J. L. G. Marinho, "Modeling and Simulation of a Horizontal Three-Phase Separator: Influence of Physicochemical Properties of Oil," *Brazilian J. Pet. Gas*, vol. 14, no. 04, pp. 205–220, 2020, https://doi.org/10.5419/bjpg2020-0016

[11] T. Ahmed, P. A. Russell, F. Hamad, and S. Gooneratne, "Experimental analysis and computational-fluid-dynamics modeling of pilot-scale three-phase separators," *SPE Prod. Oper.*, vol. 34, no. 4, pp. 805–819, 2019, https://doi.org/10.2118/197047-PA

[12] Z. Z. Khalifat, M. Zivdar, and R. Rahimi, "Application of CFD for Troubleshooting and Hydrodynamic Analysis in an Industrial Three-Phase Gravity Separator," *J. Gas Technol.*, vol. 5, no. 1, pp. 57–70, 2020. 20.1001.1.25885596.2020.5.1.6.6

[13] B. Triwibowo, H. Prasetiawan, A. Hisyam, M. F. Fauzan, and M. H. F. Rizky, "Modeling and simulation of steady state model approach for horizontal three phase separator (HTPS)," 2017, https://doi.org/10.1063/1.4976926

[14] N. Kharoua, L. Khezzar, and H. Saadawi, "CFD Modelling of a Horizontal Three-Phase Separator: A Population Balance Approach," *Am. J. Fluid Dyn.*, vol. 3, no. 4, pp. 101–118, 2013.

[15] A. P. Laleh, W. Y. Svrcek, and W. Monnery, "Computational Fluid Dynamics-Based Study of an Oilfield Separator-Part I: A Realistic Simulation," *Oil Gas Facil.*, vol. 1, no. 06, pp. 57–68, 2012, https://doi.org/10.2118/161212-pa

[16] N. Kharoua, L. Khezzar, and H. Saadawi, "Application of CFD to debottleneck production separators in a major oil field in the Middle East," *SPE Annu. Tech. Conf. Exhib.*, vol. 1, pp. 762–774, 2012, https://doi.org/10.2118/158201-ms

[17] A. P. Laleh, W. Y. Svrcek, and W. Monnery, "Computational Fluid Dynamics-Based Study of an Oilfield Separator-Part II: An Optimum Design," *Oil Gas Facil.*, vol. 2, no. 01, pp. 52–59, 2013, https://doi.org/10.2118/161036-pa

[18] A. M. Elsharkawy, "Predicting the Properties of Sour Gases and Condensates: Equations of State and Empirical Correlations," *SPE Int. Pet. Conf. Exhib. Mex.*, pp. 271–287, 2002, https://doi.org/10.2118/74369-ms

[19] D. William and Jr. McCain, *Properties of Petroleum Fluids*, Second. PennWell Publishing Company, Tusla, 1933.

[20] N. M. Al-Mhanna, "Simulation of high pressure separator used in crude oil processing," *Processes*, vol. 6, no. 11, 2018, https://doi.org/10.3390/pr6110219

[21] H. S. Naji, "Conventional and Rapid Flash Calculations for the Soave-Redlich-Kwong and Peng-Robinson Equations of State," *Emirates J. Eng. Res.*, vol. 13, no. 3, pp. 81–91, 2008.

[22] A. G. Olugbenga, N. M. Al-mhanna, M. D. Yahya, E. A. Afolabi, and M. K. Ola, "Validation of the Molar Flow Rates of Oil and Gas in Three-Phase Separators Using Aspen Hysys," *Processes*, vol. 9, no. 2, pp. 1–17, 2021, https://doi.org/10.3390/pr9020327

[23] Aspen Technology Incorporate, *Aspen HYSYS Operations Guide*. Aspen Technology, Inc. Cambridge, USA, 2005.

[24] KLM Technology Group, "Process Requirements of Vessels and Separators," in *PROJECT STANDARDS AND SPECIFICATIONS/Project Plant System*, KLM Technology Group, 2011.

[25] Iranian Ministry of Petroleum, *Engineering Standard for Process Requirements of Vessels, Reactors and Separators*. Iranian Ministry of Petroleum, 1999.

[26] M. Bothamley, "Gas/Liquids Separators: Quantifying Separation Performance - Part 2," *Oil Gas Facil.*, vol. 2, no. October, pp. 35–47, 2013.

[27] F. S. Manning and R. E. Thompson, *Oilfield Processing Volume Two: Crude Oil*. PennWell Publishing Company, Tusla, 1995.

[28] Gas Processors Suppliers Association, *Engineering Data Book*. Gas Processors Suppliers Association, Tusla, 2004.

[29] M. S. Choi, "Prediction of separator performance under changing field conditions," in *SPE Annual Technical Conference and Exhibition*, 1990, pp. 829–837, https://doi.org/10.2118/20703-ms

[30] M. Bothamley, "Gas/Liquids Separators: Quantifying Separation Performance - Part 1," *Oil Gas Facil.*, vol. 2, no. Augest, pp. 22–28, 2013. https://doi.org/10.2118/0813-0021-OGF

[31] A. Ghaffarkhah, M. A. Shahrabi, and M. K. Moraveji, "3D computational-fluid-dynamics modeling of horizontal three-phase separators: An approach for estimating the optimal dimensions," *SPE Prod. Oper.*, vol. 33, no. 4, pp. 879–895, 2018, https://doi.org/10.2118/189990-PA

اختيار الأبعاد المثلى لفاصل ذكي أفقي ثلاثي الأطوار لمحطة معالجة مكثفات الغاز في خور مور

فينك عبدالرزاق سليمان [١، *]، هيوا صديق [٢]

١ قسم هندسة البترول، كلية الهندسة، جامعة سوران، أربيل، العراق
٢ قسم هندسة البترول، كلية الهندسة، جامعة كومار للعلوم والتكنولوجيا، السليمانية، العراق

الخلاصة

تواجه محطة معالجة مكثفات الغاز في خورمور في العراق حاليًا تحديات تشغيلية بسبب مشاكل الرغوة في برج التحلية بسبب دخول السوائل الهيدروكربونية عالية الذوبان إلى البرج. قد يكون السبب الجذري للمشكلة هو تحميل السوائل حيث تفشل أوعية الفصل داخل المصنع في إزالة القطرات السائلة من الطور الغازي. لمعالجة هذه المشكلة، أجريت هذه الدراسة باستخدام برنامج أسبن هايسيس الإصدار ١١ للتحقق من أداء فاصل أفقي صناعي ثلاثي الأطوار يسمى برافو #٢، يقع قبل برج التحلية خورمور، في ظل ظروف التشغيل الحالية والمستقبلية. نتائج المحاكاة من حيث توزيع أحجام قطرات السائل في منتج الغاز وكفاءة فصل الغاز/السائل أشارت إلى أن الفاصل غير قادر على التخلص من جميع قطرات السائل ذات الأحجام المحددة من الطور الغازي لتحقيق الكفاءة المطلوبة، مع أو بدون مستخلص الرذاذ. بعد ذلك، تم تحديد وتحليل تأثير العديد من المعلمات الهيكلية للوعاء على معدل تدفق الكتلة السائلة المحملة وكفاءة وعاء الغاز/السائل. بناءً على النتائج، يوصى بمفهوم تصميم جديد يسمى "الفاصل الذكي" لبرافو #٢ تحت ظروف التشغيل الحالية والمستقبلية. أظهر الفاصل الذكي زيادة ملحوظة في كفاءة فصل الغاز/السائل، مما أدى إلى تحسين الكفاءة بنسبة ٢١,٣١٪ و ٢٤,٠٢٪ في ظل ظروف التشغيل الحالية والمستقبلية، على التوالي. يمكن أن يتحكم التصميم الذكي في ترحيل السوائل والحفاظ على مستويات عالية الكفاءة، حتى عندما تزيد معدلات تدفق مدخل الوعاء بمرور الوقت، مما يمنع ظاهرة الرغوة في المراحل السفلى بسبب السوائل المحمولة.

الكلمات الدالة: السوائل المحملة، توزيع حجم القطرات السائلة، كفاءة فصل الغاز/السائل، فاصل ذكي، لوحة قنطرة الاحتجاز القابلة للتعديل، رأس داخلي متحرك.